

Optimizing the $\text{Bi}_{2-x}\text{Sb}_x\text{Te}_{3-y}\text{Se}_y$ solid solutions to approach the intrinsic topological insulator regime

Zhi Ren, A. A. Taskin, Satoshi Sasaki, Kouji Segawa, and Yoichi Ando

Institute of Scientific and Industrial Research, Osaka University, Ibaraki, Osaka 567-0047, Japan

(Dated: October 31, 2018)

To optimize the bulk-insulating behavior in the topological insulator materials having the tetradymite structure, we have synthesized and characterized single-crystal samples of $\text{Bi}_{2-x}\text{Sb}_x\text{Te}_{3-y}\text{Se}_y$ (BSTS) solid solution at various compositions. We have elucidated that there are a series of “intrinsic” compositions where the acceptors and donors compensate each other and present a maximally bulk-insulating behavior. At such compositions, the resistivity can become as large as several Ωcm at low temperature and one can infer the role of the surface-transport channel in the non-linear Hall effect. In particular, the composition of $\text{Bi}_{1.5}\text{Sb}_{0.5}\text{Te}_{1.7}\text{Se}_{1.3}$ achieves the lowest bulk carrier density and appears to be best suited for surface transport studies.

PACS numbers: 73.25.+i, 74.62.Dh, 72.20.My, 73.20.At

I. INTRODUCTION

The three-dimensional (3D) topological insulator (TI)^{1–5} possesses spin-momentum-locked gapless surface states that are expected to host a variety of interesting quantum phenomena.^{6,7} While a number of materials have been identified to be 3D TIs,^{8–18} most of the known TI materials are poor insulators in the bulk, and finding ways to achieve a bulk-insulating state is an important current theme.^{19–25} Recently, a large bulk resistivity together with clear quantum oscillations from the surface state was observed in a ternary tetradymite TI material $\text{Bi}_2\text{Te}_2\text{Se}$ (BTS).^{26,27} In this material, the chalcogens (Te and Se) are separated into different lattice sites, forming the ordered Te-Bi-Se-Bi-Te quintuple layers. This ordering provides the chemical environment suitable for reducing defect formations.²⁶ As a result, the chalcogen-ordered tetradymite TI is a promising material for approaching the intrinsic topological-insulator regime where the bulk carriers are negligible. Since the residual bulk carrier density in BTS was found to be of the order of 10^{17} cm^{-3} ,²⁶ it is desirable to find an appropriated route to further improve the bulk-insulating properties of the chalcogen-ordered tetradymite TI material.

In this respect, the tetradymite solid solution $\text{Bi}_{2-x}\text{Sb}_x\text{Te}_{3-y}\text{Se}_y$ (BSTS) is interesting, because it has been known that some special combinations of x and y in this solid-solution system yield very low conductivity.²⁸ Except for a narrow composition region close to Sb_2Se_3 , BSTS takes the same rhombohedral structure as its three end members Bi_2Te_3 , Bi_2Se_3 , and Sb_2Te_3 , all are known to be TIs.^{11–14} Hence, BSTS is naturally expected to be a TI as long as its structure is rhombohedral. Note that the BTS compound, where a perfect chalcogen ordering is presumably achieved, can be regarded as a member of this family ($x = 0, y = 1$).

Originally, the BSTS solid solution attracted attention because of its promising thermoelectric properties for near room-temperature applications.²⁹ Decades of efforts were devoted to optimizing the thermoelectric performance through tuning the composition and/or doping

in the degenerate regime, resulting in a dimensionless figure of merit ZT ($= S^2T/\rho\kappa$, where S is the thermopower, ρ is the electrical resistivity, and κ is the thermal conductivity) close to 1. By contrast, nearly no effort was made to obtain insulating behavior in this family; nevertheless, because two prevailing types of charged defects that exist in BSTS [(Bi,Sb)/Te anti-site defects and the Se vacancy defects] introduce carriers of opposite signs, a careful tuning of x and y would, in principle, substantially cancel the bulk carriers and allow one to maximize the bulk insulating properties. In fact, based on a systematic study of polycrystalline BSTS samples at room temperature, Teramoto *et al.* inferred²⁸ that a series of such “intrinsic” compositions exist, and that the values of x and y for such compositions are linearly coupled. Unfortunately, the temperature dependence of the resistivity was not measured in their experiment, so it was not clear to what extent an insulating state was actually realized.

In the present work, we performed a systematic study of the transport properties of the BSTS solid solution for a wide range of compositions and temperature, with the aim of maximizing the insulating property. It was found that the compositions suggested by Teramoto *et al.* do not exactly correspond to the optimal compositions for insulating behavior. Instead, we determined a series of optimized compositions, where the relationship between x and y is obviously non-linear. The BSTS crystals at the optimized compositions with $0 \leq x \leq 1$ were found to present a large bulk resistivity exceeding $1\ \Omega\text{cm}$ at low temperature, and their transport properties at high temperature signify the existence of a small activation gap. This result gives evidence for the existence of a series of BSTS solid solutions where the electron and hole carriers are nearly compensated. In particular, it appears that at $(x, y) = (0.5, 1.3)$ ($\text{Bi}_{1.5}\text{Sb}_{0.5}\text{Te}_{1.7}\text{Se}_{1.3}$) the compensation is maximally realized. Although the chances of observing the Shubnikov-de Haas (SdH) oscillations in BSTS samples are not very high, one can use the non-linear Hall effect which is always observed at low temperature as a tool to infer the role of the surface-transport

channel.

II. EXPERIMENTAL DETAILS

The single crystals of $\text{Bi}_{2-x}\text{Sb}_x\text{Te}_{3-y}\text{Se}_y$ were grown by melting stoichiometric amounts of high purity elements [Bi, Sb, and Te were 6N (99.9999%), while Se was 5N (99.999%) in sealed evacuated quartz tubes at 850 °C for 48 h with intermittent shaking to ensure a homogeneity of the melt, followed by cooling slowly to 550 °C and then annealing at that temperature for 4 d. The resulting crystals have a typical domain size of up to several centimeters and are easily cleaved along the (111) plane to reveal a shiny surface. The crystal structure of each sample was investigated by the x-ray diffraction (XRD) analysis with the Cu $K\alpha$ emission, which was performed on powders obtained by crushing the crystals. Lattice parameters were refined by a least-squares fitting to the XRD data with the consideration of the zero shifts. All the samples used for transport measurements were confirmed to be single domain by using the x-ray Laue analysis, and they were cut into thin bar-shaped specimens with the typical thickness of 100 μm . The in-plane resistivity ρ_{xx} and the Hall resistivity ρ_{yx} were measured by using the standard six-probe method in a Quantum Design Physical Properties Measurement System (PPMS-9) down to 1.8 K, shortly after the electrical contacts were prepared by using room-temperature-cured silver paste.

III. INTRINSIC COMPOSITIONS

Figures 1(a)-(c) present how the compositions of the solid solution were optimized for the insulating behavior. Initially, we synthesized and characterized samples for the “intrinsic” compositions suggested in Ref. 28. However, it turned out that, except for the $(x, y) = (0.5, 1.3)$ case, all those samples were only poorly insulating or even metallic, with a nearly T -independent Hall coefficient signifying the existence of electron carriers with the density of 10^{18} – 10^{19} cm^{-3} , which indicated that there are too much Se vacancies that are not sufficiently compensated by the (Bi,Sb)/Te anti-site defects. Therefore, we tried to optimize the composition by increasing the Se content y while fixing the Sb content x . The examples for $x = 0$ and 1 are shown in Figs. 1(a) and (b). We have also performed similar optimization along the structural phase boundary [line A-B in Fig. 1(d)], in which one must simultaneously vary the values of x and y . As shown in Fig. 1(c), the composition $(x, y) = (1.5, 2.4)$ suggested in Ref. 28 yielded only metallic samples; moving to $(x, y) = (1.4, 2.44)$ was not sufficient, and finally at $(x, y) = (1.25, 2.5)$ we found an insulating behavior.

The summary of the optimized compositions are shown in the composition-structure diagram [Fig. 1(d)], together with the linear “intrinsic” composition line suggested in Ref. 28. The possible errors in our experiment,

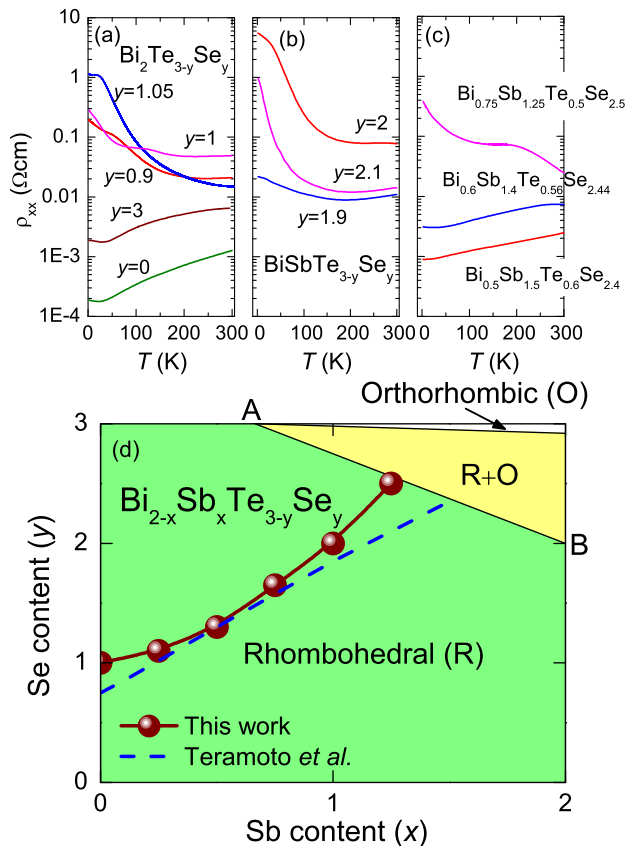


FIG. 1: (Color online) (a,b) Temperature dependences of ρ_{xx} for BSTS samples with fixed x and different y , showing how the compositions were optimized for the insulating behavior; panel (a) is for $x = 0$ ($\text{Bi}_2\text{Te}_{3-y}\text{Se}_y$) and panel (b) is for $x = 1$ ($\text{BiSbTe}_{3-y}\text{Se}_y$). (c) $\rho_{xx}(T)$ data used for optimizing the composition along the structural phase boundary [line A-B in panel (d)]. (d) Composition-structure diagram of the $\text{Bi}_{2-x}\text{Sb}_x\text{Te}_{3-y}\text{Se}_y$ system. The circles denote the “intrinsic” compositions determined in the present work, while the dashed line denotes those suggested in Ref. 28. This diagram was determined by first fixing the Sb content x and optimizing the Se content y for that x ; the possible error in the optimized y value for a given x is the step size in the optimization process and is represented by the symbol size.

which mostly come from the finite step size in the optimization process, are represented by the symbol size. Obviously, the relationship between x and y in the true “intrinsic” compositions is not linear but shows an upward curvature in this diagram. It should be noted that Teramoto *et al.* used polycrystalline samples and only measured the conductivity at room temperature;²⁸ it is therefore not surprising that the present result does not agree with their conclusion.

IV. CRYSTAL STRUCTURE

Figure 2(a) shows the powder XRD patterns for the series of BSTS solid solutions at the optimized composi-

TABLE I: Important parameters obtained for the optimized compositions. Δ and Δ^* are the thermal activation energies determined from the temperature dependences of ρ_{xx} and R_H , respectively. The effective acceptor concentration N_A^{eff} is estimated from the relation $R_H^{-1} \approx e\sqrt{N_A^{\text{eff}}N_V} \exp(-\Delta^*/k_B T)$, where $N_V = 5.2 \times 10^{18} \text{ cm}^{-3}$ (Ref. 26) was assumed. Note that, among the samples with the same composition, Δ and Δ^* vary by $\sim 10\%$ and N_A^{eff} could vary by a factor of three, probably due to different levels of defect concentrations.

composition	a (Å)	c (Å)	$\rho_{xx}^{300\text{K}}$ (mΩcm)	$\rho_{xx}^{1.8\text{K}}$ (Ωcm)	$R_H^{300\text{K}}$ (cm ³ /C)	$R_H^{1.8\text{K}}$ (cm ³ /C)	Δ (meV)	Δ^* (meV)	N_A^{eff} (cm ⁻³)
Bi ₂ Te _{1.95} Se _{1.05}	4.28	29.86	14	1.1	2.6	-200	22	33	9×10^{18}
Bi _{1.75} Sb _{0.25} Te _{1.85} Se _{1.15}	4.26	29.84	25	2.1	2.3	-610	43	60	5×10^{19}
Bi _{1.5} Sb _{0.5} Te _{1.7} Se _{1.3}	4.24	29.83	140	4.5	2.7	-910	53	65	6×10^{19}
Bi _{1.25} Sb _{0.75} Te _{1.3} Se _{1.7}	4.20	29.58	44	2.2	2.7	-370	38	48	2×10^{19}
BiSbTeSe ₂	4.16	29.41	77	5.5	2.4	802	30	22	1×10^{18}
Bi _{0.75} Sb _{1.25} Te _{0.5} Se _{2.5}	4.12	29.16	25	0.38	-10.6	207	—	—	—

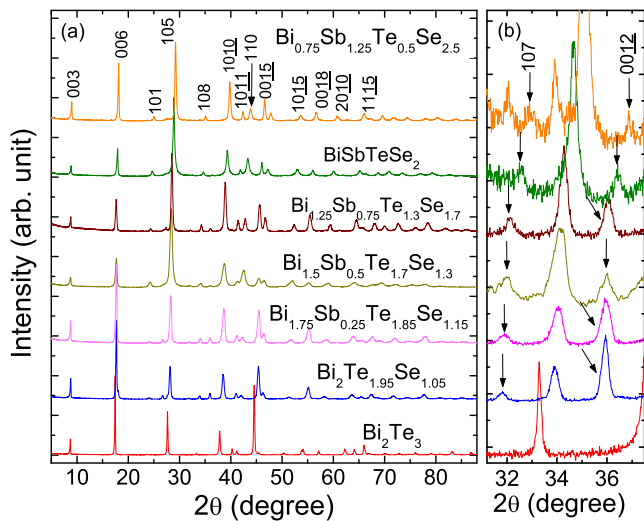


FIG. 2: (Color online) (a) Power XRD patterns for the series of BSTS samples at optimized compositions. The pattern for Bi₂Te₃ is also shown for comparison. All the diffraction peaks can be indexed based on the rhombohedral structure with the $R\bar{3}m$ space group. (b) Enlarged view of the data near the (108) peak. Arrows mark the (107) and (0012) peaks related to the ordering of the chalcogen layers.

tions, together with the Bi₂Te₃ data which is shown for comparison. The patterns for all the samples are essentially the same and can be well indexed with the rhombohedral structure (space group $R\bar{3}m$), confirming that the solid solutions maintain the same crystal structure as their binary end members Bi₂Te₃, Bi₂Se₃, and Sb₂Te₃. The refined lattice parameters are summarized in Table I. As the system moves toward Sb₂Se₃, both the a and c lattice parameters tend to decrease, which is reasonable because the ionic radius of Sb (Se) is smaller than that of Bi (Te).

It is important to note that the (107) and (0012) peaks, both of which are characteristic of the compounds with the BTS-type chalcogen ordering, are present in all the BSTS samples, as can be seen in the magnified

plot [Fig. 2(b)]. This indicates that the ordering of the chalcogen layers is preserved to some extent despite a large change in stoichiometry. To understand this observation, it is useful to recall the structure of the tetradymite, which is composed of stacked $A_2^V B_3^{VI}$ ($A^V = \text{Bi, Sb}; B^{VI} = \text{Te, Se}$) quintuple layers. Within the quintuple layer, the atoms are arranged in the sequence of $B^{VI}(1)-A^V-B^{VI}(2)-A^V-B^{VI}(1)$, where $B^{VI}(1)$ and $B^{VI}(2)$ are two inequivalent crystallographic sites. Because Se has a larger electronegativity than Te, the Se atoms preferentially occupy the $B^{VI}(2)$ site and the remaining $(y-1)\text{Se} + (3-y)\text{Te}$ atoms are distributed randomly in the $B^{VI}(1)$ site when y is larger than 1.³⁰ Such an asymmetric arrangement of the chalcogen layers bears similarity to that in BTS and accounts for the XRD results.

V. RESISTIVITY

Figure 3(a) shows the typical temperature dependences of ρ_{xx} for the optimized compositions. It should be noted that the ρ_{xx} value was found to be sample dependent and could vary by a factor of three within the same composition, probably due to different levels of defect concentrations. Nevertheless, the activated behavior was essentially reproducible within the same batch and the variation in terms of the activation energy was about 10%. The magnitude of ρ_{xx} at room temperature in Fig. 3(a) ranges from 25 to 140 mΩcm, which is generally larger than that found in BTS.²⁶ Except for the $(x, y) = (1.25, 2.5)$ composition which has the largest Se content, the overall temperature dependence of ρ_{xx} is similar and can be divided into three regimes:

(i) *Activated regime*: In the temperature range above ~ 100 K, the $\rho_{xx}(T)$ data can be fitted with the Arrhenius law

$$\rho_{xx} \sim \exp(\Delta/k_B T), \quad (1)$$

where Δ is the activation energy and k_B is the Boltzmann constant. In Fig. 3(b), we show the Arrhenius plot of

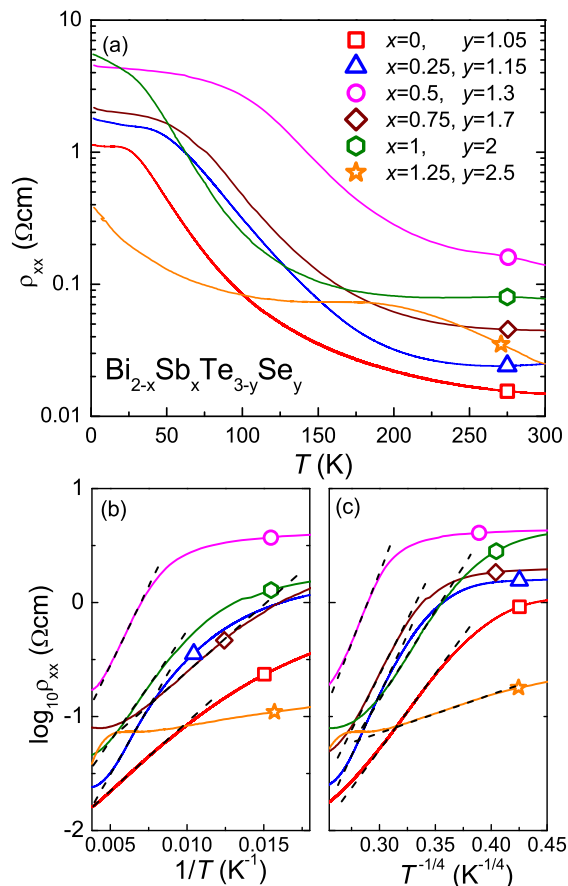


FIG. 3: (Color online) (a) Temperature dependences of ρ_{xx} for the series of BSTS samples at optimized compositions. Note that the vertical axis is in the logarithmic scale with base 10. (b) and (c) are the Arrhenius plot [$\log_{10} \rho_{xx}$ vs $1/T$] and the 3D-VRH plot [$\log_{10} \rho_{xx}$ vs $T^{-1/4}$] of the $\rho_{xx}(T)$ data, respectively. Dashed lines represent linear fittings to the regions where the activation and the VRH behaviors can be recognized.

the data together with linear fittings to obtain Δ . The Δ values are summarized in Table I, and they vary from 22 to 53 meV; however, since the temperature range of this activated behavior is not very wide, the obtained Δ should not be taken too literally.

(ii) *Variable-range hopping regime*: Below the temperature range of the activated behavior mentioned above, the $\rho_{xx}(T)$ appears to be better described by the 3D variable-range hopping (VRH) behavior,

$$\rho_{xx} \sim \exp[(T/T_0)^{-1/4}], \quad (2)$$

where T_0 is a constant which depends on the density of states at the Fermi level E_F . For example, in the data for $\text{Bi}_2\text{Te}_{1.95}\text{Se}_{1.05}$ (marked by square in Fig. 3), the VRH behavior holds for 60 – 140 K, while the activated behavior holds for 110 – 300 K. However, it should be noted that the temperature range where this VRH behavior appears to hold can have a significant overlap with the

activated temperature range. For example, in the case of $\text{Bi}_{1.25}\text{Sb}_{0.75}\text{Te}_{1.3}\text{Se}_{1.7}$ (marked by diamond in Fig. 3) where the distinction is the most ambiguous, the activation behavior and the VRH behavior appear to hold in similar ranges, 85 – 140 K and 90 – 170 K, respectively. Hence, the distinction between the two transport mechanisms can be a subtle issue, and it probably depends on the level of disorder in the sample.

(iii) *Saturation regime*: At low temperature, ρ_{xx} tends to saturate, rather than to diverge as expected for intrinsic semiconductors, implying the existence of some extended states at E_F in the zero-temperature limit. In this regime, the magnetic-field dependence of the Hall resistivity ρ_{yx} is generally non-linear (as will be described in detail later), which points to the existence of two or more transport channels. In the BTS compound, it was elucidated²⁶ that the topological surface state and a degenerate bulk impurity band both contribute to the low-temperature saturated resistivity. In addition, our recent study of the $\text{Bi}_{1.5}\text{Sb}_{0.5}\text{Te}_{1.7}\text{Se}_{1.3}$ compound has identified³¹ the third contribution of the accumulation layer (which is caused by the surface band bending and is topologically trivial) in samples where the Hall coefficient is positive at low temperature.

VI. HALL COEFFICIENT

To further characterize the transport properties, we have performed the Hall measurements. Figure 4(a) shows the temperature dependences of the low-field Hall coefficient R_H , defined as $R_H = \rho_{yx}/B$ near $B = 0$, for the same series of samples. Above ~ 150 K, ρ_{yx} is always linear in B so that ρ_{yx}/B is magnetic-field independent, and the resulting R_H is positive and shows a thermally-activation behavior in all the BSTS samples except $\text{Bi}_{0.75}\text{Sb}_{1.25}\text{Te}_{0.5}\text{Se}_{2.5}$. The positive and activated $R_H(T)$ behavior indicates that the dominant charge carriers are thermally-excited holes in the bulk valence band. By contrast, the high-temperature R_H in $\text{Bi}_{0.75}\text{Sb}_{1.25}\text{Te}_{0.5}\text{Se}_{2.5}$ is negative and only weakly dependent on temperature, which indicates that the electron carriers created by Se vacancies in this compound are degenerate near room temperature. Thus, the sign change in the high-temperature R_H at the largest Se content y in our series of samples reflects a change in the dominant defects from the Bi(Sb)/Te anti-sites (acceptors) to the Se vacancies (donors). Note that in those samples both acceptors and donors are expected to exist, and the observed charge-carrier concentration is likely to be determined by their competition.

From the Arrhenius plot of $R_H(T)$ [Fig. 4(b)], one obtains the effective acceptor concentration N_A^{eff} together with the effective activation energy Δ^* , both are summarized in Table I. It should be noted that, among the samples with the same composition, the variation in Δ^* was within $\sim 10\%$, while N_A^{eff} could vary up to a factor of three, reflecting the variation in the resistivity behavior

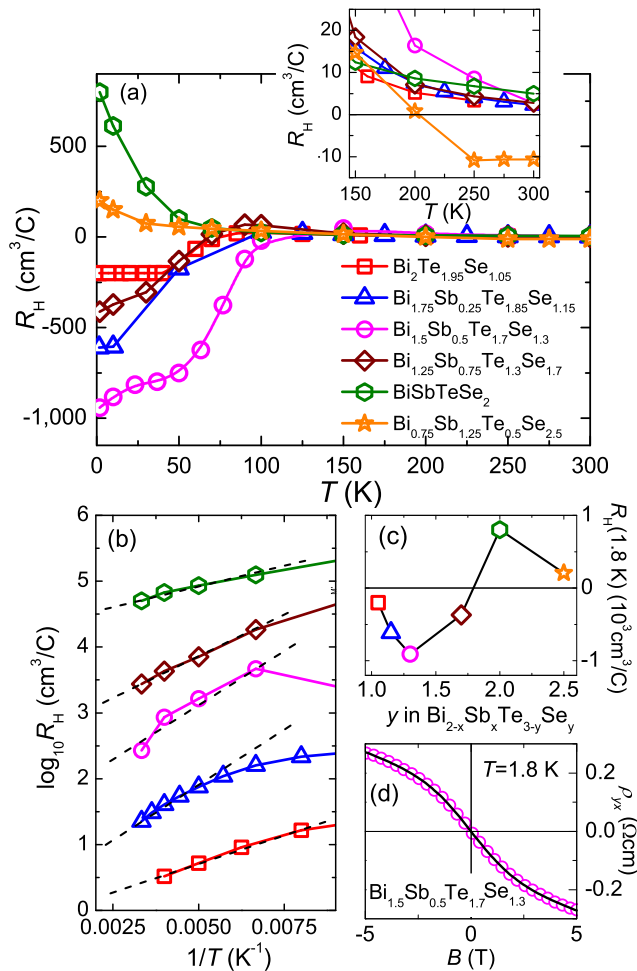


FIG. 4: (Color online) (a) Temperature dependences of the low-field Hall coefficient R_H for the series of BSTS samples at optimized compositions. Inset shows an enlarged view of the data between 150 and 300 K. (b) Arrhenius plot of $R_H(T)$ at high temperature for the series of samples except $\text{Bi}_{0.75}\text{Sb}_{1.25}\text{Te}_{0.5}\text{Se}_{2.5}$ where the activation behavior was not clearly observed; the data are shifted vertically for clarity. Dashed lines are the Arrhenius-law fittings to extract the activation energy Δ^* . (c) The value of R_H at 1.8 K plotted as a function of the Se content y . (d) Magnetic-field dependence of ρ_{yx} for the $\text{Bi}_{1.5}\text{Sb}_{0.5}\text{Te}_{1.7}\text{Se}_{1.3}$ sample at 1.8 K; solid line is a two-band-model fitting (Ref. 26) to the data. The obtained fitting parameters give the surface conductance of $1.4 \times 10^{-4} \Omega^{-1}$ and the bulk conductivity of $0.21 \Omega^{-1}\text{cm}^{-1}$; since the measured sample was 120 μm thick, the surface contribution was 5% of the total conductance.

within the same batch mentioned in Sec. V. One can see that the Δ^* values are not much different from the Δ values derived from the $\rho_{xx}(T)$ data for the same samples, and the difference is less than 30%. This small differences can probably be ascribed to the temperature dependence of the mobility. Intriguingly, N_A^{eff} and Δ^* seem to be correlated; namely, larger N_A^{eff} is accompanied with larger Δ^* . However, the origin of this behavior is not clear at

the moment.

At lower temperature below 100 K, $\rho_{yx}(B)$ is no longer a linear function of B and R_H becomes very much dependent on composition. Figure 4(c) shows this variation in terms of the R_H value at 1.8 K plotted vs y .³² The largest $|R_H|$ was observed in $\text{Bi}_{1.5}\text{Sb}_{0.5}\text{Te}_{1.7}\text{Se}_{1.3}$, where $R_H = -910 \text{ cm}^2/\text{C}$ at 1.8 K. This value would naively correspond to a very low carrier density of $7 \times 10^{15} \text{ cm}^{-3}$; however, as we have demonstrated for BTS,²⁶ such a naive estimate based on the low-field R_H is not reliable when there are multiple transport channels that cause $\rho_{yx}(B)$ to become non-linear. Indeed, $\rho_{yx}(B)$ was found to be non-linear in $\text{Bi}_{1.5}\text{Sb}_{0.5}\text{Te}_{1.7}\text{Se}_{1.3}$ [Fig. 4(d)], and an accurate estimate of the bulk and surface carrier densities is difficult without employing additional information from SdH oscillations.^{26,33} Nevertheless, by using the simple two-band model to consider both the bulk and surface transport channels²⁶ (note that the accumulation layer³¹ is irrelevant here since the slope of $\rho_{yx}(B)$ is negative), one can make a reasonable fitting to the data [solid line in Fig. 4(d)], which yields the bulk carrier density $1.8 \times 10^{16} \text{ cm}^{-3}$, the bulk mobility $73 \text{ cm}^2/\text{Vs}$, the surface carrier density $1.5 \times 10^{11} \text{ cm}^{-2}$, and the surface mobility $2900 \text{ cm}^2/\text{Vs}$. (In the fitting procedure, the parameters were constrained by the measured ρ_{xx} value in 0 T.) Based on this fitting result one can estimate the contribution of the surface transport to the total conductance to be $\sim 5\%$, which is reasonably large considering the thickness (120 μm) of the measured sample.

VII. DISCUSSIONS

For the transport studies of the topological surface states, it is desirable that their SdH oscillations are observed. In the present series of BSTS samples, we did not observe clear SdH oscillations below 9 T. Most likely, whether the SdH oscillations can be observed depends crucially on the homogeneity and the value of the surface carrier density n_s ,³⁴ which may vary between samples and, even in the same single crystal, between different cleaves. The chances of observing the SdH oscillations were roughly 10% in our BSTS samples. On such lucky occasions, we were able to see both Dirac holes and electrons on the surface of $\text{Bi}_{1.5}\text{Sb}_{0.5}\text{Te}_{1.7}\text{Se}_{1.3}$ samples, and the result was reported in Ref. 31. It should be emphasized, however, that even though the SdH oscillations are not always observed, one can achieve a surface-dominated transport by making sufficiently thin samples of BSTS.³¹

As we have already discussed in Sec. VI, the low-field R_H value in BSTS does not simply reflect the bulk carrier density, but it is also influenced by the contribution of the surface carriers which presumably have a higher mobility than the bulk carriers. In view of this situation, the non-trivial composition dependence of R_H observed at 1.8 K [Fig. 4(c)] can be interpreted in two ways: One possibility is that it may signify the sign change of the surface carriers as the Se concentration y is increased. This is

possible because the surface band structure of BTS is similar¹⁸ to that of Bi₂Te₃ where the Dirac point is located below the top of the valence band,¹³ whereas with increasing y the surface band structure is expected to approach that of Bi₂Se₃ where the Dirac point is isolated in the bulk gap;¹² therefore, if the chemical potential is pinned to the impurity band located just above the bulk valence band,²⁶ the nature of the surface carriers could change from Dirac electrons to Dirac holes. The other possibility is that the change in R_H is a reflection of the change in the nature of the degenerate bulk carriers in the impurity band. This is also possible because at low y the chemical potential is likely to be located below the center of the acceptor impurity band, whereas with increasing y the increasing amount of donors (due to Se vacancies) would cause the acceptor impurity band to be gradually filled and move the chemical potential to above the center of the impurity band. To further address this issue, systematic studies employing the SdH oscillations would be necessary.

VIII. CONCLUSION

In this work, we have elucidated in the Bi_{2-x}Sb_xTe_{3-y}Se_y (BSTS) solid solution the existence of the “intrinsic” compositions where the acceptors due to the (Bi,Sb)/Te anti-site defects and the donors due to the Se vacancy defects compensate each other and realize

a maximally bulk-insulating state. The powder XRD patterns suggest that at those compositions optimized for the insulating behavior, the crystal structure has an ordering of the chalcogen layers in which the Se atoms preferentially occupy the middle of the quintuple layer and the remaining Se and Te atoms randomly occupy the outer-most layers. Except for Bi_{0.75}Sb_{1.25}Te_{0.5}Se_{2.5} which is close to the structural instability, all the BSTS samples at the optimized compositions show large ρ_{xx} values exceeding 1 Ωcm at low temperature, together with an activated behavior at high temperature signifying the existence of an activation gap for the bulk carriers. The B dependence of ρ_{yx} at low temperature points to the role of the surface transport channel, and the non-trivial composition dependence of the low-field R_H reflects either the change in the surface band structure or the change in the bulk carriers in the impurity band. The $|R_H|$ value at 1.8 K was found to be the largest in Bi_{1.5}Sb_{0.5}Te_{1.7}Se_{1.3} and this composition appears to have achieved the lowest bulk carrier density.

Acknowledgments

This work was supported by JSPS (NEXT Program), MEXT (Innovative Area “Topological Quantum Phenomena” KAKENHI 22103004), and AFOSR (AOARD 10-4103).

-
- ¹ L. Fu, C. L. Kane, and E. J. Mele, Phys. Rev. Lett. **98**, 106803 (2007).
² J.E. Moore and L. Balents, Phys. Rev. B **75**, 121306(R) (2007).
³ R. Roy, Phys. Rev. B **79**, 195322 (2009).
⁴ L. Fu and C.L. Kane, Phys. Rev. B **76**, 045302 (2007).
⁵ X-L. Qi, T. L. Hughes, and S.-C. Zhang, Phys. Rev. B **78**, 195424 (2008).
⁶ M.Z. Hasan and C.L. Kane, Rev. Mod. Phys. **82**, 3045 (2010).
⁷ X.L. Qi and S.C. Zhang, Rev. Mod. Phys. (to be published).
⁸ D. Hsieh, D. Qian, L. Wray, Y. Xia, Y.S. Hor, R.J. Cava, and M.Z. Hasan, Nature **452**, 970 (2008).
⁹ A.A. Taskin and Y. Ando, Phys. Rev. B **80**, 085303 (2009).
¹⁰ A. Nishide, A.A. Taskin, Y. Takeichi, T. Okuda, A. Kakizaki, T. Hirahara, K. Nakatsuji, F. Komori, Y. Ando, and I. Matsuda, Phys. Rev. B. **81**, 041309(R) (2010).
¹¹ H.-J. Zhang, C.-X. Liu, X.-L. Qi, X. Dai, Z. Fang, and S.-C. Zhang, Nat. Phys. **5**, 438 (2009).
¹² Y. Xia, D. Qian, D. Hsieh, L. Wray, A. Pal, H. Lin, A. Bansil, D. Grauer, Y.S. Hor, R.J. Cava, and M.Z. Hasan, Nat. Phys. **5**, 398 (2009).
¹³ Y.L. Chen, J.G. Analytis, J.-H. Chu, Z.K. Liu, S.-K. Mo, X.L. Qi, H.J. Zhang, D.H. Lu, X. Dai, Z. Fang, S.C. Zhang, I.R. Fisher, Z. Hussain, and Z.-X. Shen, Science **325**, 178 (2009).
¹⁴ D. Hsieh, Y. Xia, D. Qian, L. Wray, F. Meier, J. H. Dil, J. Osterwalder, L. Patthey, A. V. Fedorov, H. Lin, A. Bansil, D. Grauer, Y. S. Hor, R. J. Cava, and M. Z. Hasan, Phys. Rev. Lett. **103**, 146401 (2009).
¹⁵ T. Sato, K. Segawa, H. Guo, K. Sugawara, S. Souma, T. Takahashi, and Y. Ando, Phys. Rev. Lett. **105**, 136802 (2010).
¹⁶ K. Kuroda, M. Ye, A. Kimura, S.V. Eremeev, E.E. Krasovskii, E.V. Chulkov, Y. Ueda, K. Miyamoto, T. Okuda, K. Shimada, H. Namatame, and M. Taniguchi, Phys. Rev. Lett. **105**, 146801 (2010).
¹⁷ Y.L. Chen, Z.K. Liu, J.G. Analytis, J.-H. Chu, H.J. Zhang, B.H. Yan, S.-K. Mo, R.G. Moore, D.H. Lu, I.R. Fisher, S.-C. Zhang, Z. Hussain, and Z.-X. Shen, Phys. Rev. Lett. **105**, 266401 (2010).
¹⁸ S.Y. Xu, L.A. Wray, Y. Xia, R. Shankar, A. Petersen, A. Fedorov, H. Lin, A. Bansil, Y.S. Hor, D. Grauer, R.J. Cava, and M.Z. Hasan, arXiv:1007.5111v1.
¹⁹ D.-X. Qu, Y.S. Hor, J. Xiong, R.J. Cava, and N.P. Ong, Science **329**, 821 (2010).
²⁰ J.G. Analytis, R.D. McDonald, S.C. Riggs, J.-H. Chu, G.S. Boebinger, and I.R. Fisher, Nat. Phys. **10**, 960-964 (2010).
²¹ J.G. Checkelsky, Y.S. Hor, M.-H. Liu, D.-X. Qu, R.J. Cava, and N.P. Ong, Phys. Rev. Lett. **103**, 246601 (2009).
²² N.P. Butch, K. Kirshenbaum, P. Syers, A.B. Sushkov, G.S. Jenkins, H.D. Drew, and J. Paglione, Phys. Rev. B **81**, 241301 (2010).
²³ J.G. Analytis, J.H. Chu, Y. Chen, F. Corredor, R.D. McDonald, Z.X. Shen, and I.R. Fisher, Phys. Rev. B **81**,

- 205407 (2010).
- ²⁴ K. Eto, Z. Ren, A.A. Taskin, K. Segawa, and Y. Ando, Phys. Rev. B **81**, 195309 (2010).
- ²⁵ Z. Ren, A.A. Taskin, S. Sasaki, K. Segawa, and Y. Ando, Phys. Rev. B **84**, 075316 (2011).
- ²⁶ Z. Ren, A.A. Taskin, S. Sasaki, K. Segawa, and Y. Ando, Phys. Rev. B **82**, 241306(R) (2010).
- ²⁷ J. Xiong, A.C. Petersen, D.X. Qu, R.J. Cava, and N.P. Ong, arXiv:1101.1315.
- ²⁸ I. Teramoto and S. Takayanagi, J. Phys. Chem. Solids **19**, 124 (1961).
- ²⁹ L.R. Testardi, J.N.Jr. Bierly, and F.J. Donahoe, J. Phys. Chem. Solids **23**, 1209 (1962); C.H. Champness, P.T. Chiang, and P. Parekh, Can. J. Phys. **43**, 653 (1965); H.W. Jeon, H.P. Ha, D.B. Hyun, and J.D. Shim, J. Phys. Chem. Solids **52**, 579 (1991).
- ³⁰ S. Nakajima, J. Phys. Chem. Solids **24**, 479 (1963).
- ³¹ A.A. Taskin, Z. Ren, S. Sasaki, K. Segawa, and Y. Ando, Phys. Rev. Lett. **107**, 016801 (2011).
- ³² In our recent study of $\text{Bi}_{1.5}\text{Sb}_{0.5}\text{Te}_{1.7}\text{Se}_{1.3}$, we observed that in very thin samples the low-temperature R_H can be positive immediately after the cleavage, and it changes sign with time (Ref. 31). All the samples measured in the present work were relatively thick ($\sim 100 \mu\text{m}$) and did not show clear time evolution in R_H .
- ³³ A.A. Taskin, K. Segawa, and Y. Ando, Phys. Rev. B **82**, 121302(R) (2010).
- ³⁴ When n_s is inhomogeneous, the SdH oscillation frequency varies across the sample and the oscillations are smeared; also, when n_s is too small, the SdH oscillation frequency becomes too low to be detected in our limited magnetic-field range.